

Construction of A Novel Ferroptosis-related Prognostic Risk Signature for Survival Prediction in Clear Cell Renal Cell Carcinoma Patients

Fucaï Tang^{1*}, Jiahao Zhang^{2*}, Langjing Zhu^{3*}, Yongchang Lai¹, Zhibiao Li⁴, Zeguàng Lu⁵, Zhicheng Tang⁴, Yuexue Mai², Rende Huang⁶, Zhaohui He¹

Purpose: Targeted ferroptosis is a reliable therapy to inhibit tumor growth and enhance immunotherapy. This study generated a novel prognostic risk signature based on ferroptosis-related genes (FRGs), and explored the ability in clinic for clear cell renal cell carcinoma (ccRCC).

Materials and Methods: The expression profile of mRNA and FRGs for ccRCC patients were exacted from The Cancer Genome Atlas (TCGA) database. A ferroptosis-related prognostic risk signature was constructed based on univariable and multivariable Cox-regression analysis. Kaplan-Meier (KM) survival curves and receiver operating characteristic (ROC) curves were performed to access the prognostic value of riskscore. A nomogram integrating riskscore and clinical features was established to predict overall survival (OS). Based on differentially expressed genes between high- and low-OS groups with 5-year OS, function enrichment analyses and single-sample gene set enrichment analysis (ssGSEA) were investigated to immune status.

Results: A 9-FRGs prognostic risk signature was constructed based on 37 differentially expressed FRGs. ROC and KM curves showed that riskscore has excellent reliability and predictive ability; Cox regression disclosed the riskscore as an independent prognosis for ccRCC patients. Then, the C-index and calibration curve demonstrated the good performance of the nomogram in the training and validation cohort, and its predictive ability better than other features. Immune-related biological processes were enriched by function enrichment analysis, and the immune-related cells and functions were differential by ssGSEA between high- and low-OS groups.

Conclusion: Our study identified and verified a novel 9-FRGs prognostic signature and nomogram to predict OS, providing a novel sight to explore targeted therapy of ferroptosis for ccRCC.

Keywords: clear cell renal cell carcinoma; ferroptosis; immunity; prognosis; nomogram; survival

INTRODUCTION

Renal cell carcinoma (RCC) is one of the ten most common cancers in the world, which accounts for more than 90% of all renal cell carcinoma types, ranking sixth in men and tenth in women, and clear cell renal cell carcinoma (ccRCC) is the most common subtype of RCC, of which ccRCC is 75% of RCC.^(1,2) At present, the research showed that the risk factors for RCC are smoking, obesity, hypertension, and chronic kidney disease.⁽¹⁾ In recent years, there has been a broad advance in the development of treatments for ccRCC, including targeted therapy, chemotherapy, and immunotherapy, of which therapy of immune checkpoint inhibitors is considered a more effective therapy for ccRCC patients.

⁽³⁾ However, the targets of immune therapy still need to be supplemented and improved. In addition, most patients with ccRCC are diagnosed in the advanced stage, because the early-phase symptoms of ccRCC are not apparent and TNM staging is not an effective predictor of early ccRCC.⁽⁴⁾ Therefore, it is essential to evaluate the prognosis of ccRCC precisely. Meanwhile, the need for accurate biomarkers still has not been met plus the high heterogeneity of ccRCC.⁽¹⁾ As a new nonapoptotic form of cell death based on regulated necrosis by the iron-dependent lipid peroxidation, ferroptosis has different properties in morphology and biochemistry as well as gene signature compared to apoptosis, necrosis, and autophagy.^(5,6) Ferroptosis is primarily due to the accumulation of cellular reactive

¹Department of Urology, The Eighth Affiliated Hospital, Sun Yat-sen University, Shenzhen, Guangdong, 518033, China.

²The Sixth Clinical College of Guangzhou Medical University, Guangzhou, Guangdong, 511436, China.

³Department of Nephrology, The Eighth Affiliated Hospital, Sun Yat-sen University, Shenzhen, 518033, China.

⁴The Third Clinical College of Guangzhou Medical University, Guangzhou, Guangdong, 511436, China.

⁵The Second Clinical College of Guangzhou Medical University, Guangzhou, Guangdong, 511436, China.

⁶The KindMed School of Laboratory Medicine of Guangzhou Medical University, Guangzhou, Guangdong, 511436, China.

* Fucaï Tang, Jiahao Zhang, and Lang-Jing Zhu contributed equally to this work.

*Correspondence: Department of Urology, The Eighth Affiliated Hospital, Sun Yat-sen University, Shennan Zhong Road #3025, Futian District, Shenzhen, 518033 Guangdong, China. E-mail address: hechh9@mail.sysu.edu.cn.

Received September 2021 & Accepted April 2022

Table 1. Baseline clinicopathological features of patients with ccRCC

Variables	Training cohort (n=251)	Validation cohort (n=251)	Total (n=502)	P-value
Gender				.452
Male	82 (32.7)	90 (35.9)	172 (34.3)	
Female	169 (67.3)	161 (64.1)	330 (65.7)	
Age (years)	59.4 ± 12.5	61.1 ± 11.9	60.3 ± 12.1	.230
Grade				.324
G1/G2	109 (43.4)	120 (47.8)	229 (45.6)	
G3/G4	142 (56.6)	131 (52.2)	273 (54.4)	
Stage				.584
Stage I	125 (49.8)	126 (50.2)	251 (50.0)	
Stage II	28 (11.2)	25 (10.0)	53 (10.6)	
Stage III	62 (24.7)	54 (21.5)	116 (23.1)	
Stage IV	36 (14.3)	46 (18.3)	82 (16.3)	
Status				.776
Alive	169 (67.3)	166 (66.1)	335 (66.7)	
Dead	82 (32.7)	85 (33.9)	167 (33.3)	

^aData are presented as mean ± SD or number (percent)

oxygen species (ROS) caused by lipid peroxidation exceeding the scavenging power of ROS that bases on the redox ability maintained by phospholipid hydroperoxidase and glutathione (GSH), and specifically, the reason for ferroptosis is divided to the cysteine deprivation-caused ferroptosis and phospholipid glutathione peroxidase 4 (GPX4) inhibition-induced ferroptosis.^(5,7) And ferroptosis is not only intimately correlated to lots of biological metabolic processes, such as the metabolism of amino acid, iron, polyunsaturated fatty acid, and biosynthesis soon, but also related to a variety of disease processes, especially breast cancer, renal cell carcinoma, and liver cancer so on.^(5,8) Ferroptosis-induction combination with immunotherapy is becoming a new alternative therapeutic method for cancer gradually.⁽⁹⁾ The latest research exhibited, as the vital tumor suppressor in ccRCC, VHL can decrease the lipid storage and highly express relevant genes of oxidative phosphorylation and fatty acid metabolism to promote ferroptosis. The other side of the shield, GS, GLS, GCLC, GCLM, and SLC7A11 were positively correlated with ferroptosis in ccRCC.⁽¹⁰⁾ These corresponding genes are about glutathione metabolism. However, the relationship between these genes and prognosis is still unknown, and we still need to find more relevant ferroptosis-genes about the prognosis of ccRCC patients. In this study, we analyzed the ferroptosis-related genes

(FRGs) to complete the construction and validation of the novel prognostic multi-gene signature for ccRCC patients in the TCGA cohort. Then, combined with clinical information and risk score, the nomogram was constructed and validated. Finally, to reveal the potential mechanism, function enrichment analysis and ssGSEA score of immune status were performed. We presented the following article/case in accordance with the transparent reporting of a multivariable prediction model for individual prognosis or diagnosis (TRIPOD) reporting checklist (<https://www.equator-network.org/reporting-guidelines/tripod-statement/>).

MATERIALS AND METHODS

Data Acquisition and Study Population

A brief flow chart to study design is shown in Supplementary Figure S1. The RNA sequencing expression profile and relevant clinical information for ccRCC patients were downloaded and exacted from The Cancer Genome Atlas (TCGA, <https://cancergenome.nih.gov/>, Date: September 18, 2020 to January 20, 2021). Specifically, for inclusion criteria, these included patients must have complete clinical information, including age, gender, tumor grades, tumor stages, follow-up time, and survival status. For exclusion criteria, patients with less than one month in follow-up and missing clinical information were excluded. Ultimately, 502 ccRCC tissue

Table 2. Univariable and multivariable Cox regression analysis for OS in ccRCC patients from the training cohort

Variables	Univariable Cox analysis			Multivariable Cox analysis		
	HR	95%CI	P-value	HR	95%CI	P-value
Gender						
Male	Reference			Reference		
Female	0.95	0.60-1.50	.827			
Age	1.02	1.00-1.04	.039	1.02	1.00-1.04	.121
Grade						
G1/G2	Reference			Reference		
G3/G4	2.64	1.60-4.38	< .001	1.41	0.81-2.45	.224
Stage				Reference		
Stage I	Reference			Reference		
Stage II	1.10	0.44-2.72	.839	0.92	0.37-2.30	.854
Stage III	2.46	1.38-4.40	.002	1.54	0.81-2.83	.199
Stage IV	8.85	5.05-15.51	< .001	4.67	2.45-8.80	< .001
Riskscore	2.72	2.10-3.52	< .001	2.11	1.58-2.80	< .001

Abbreviations: HR, Hazard Ratio.

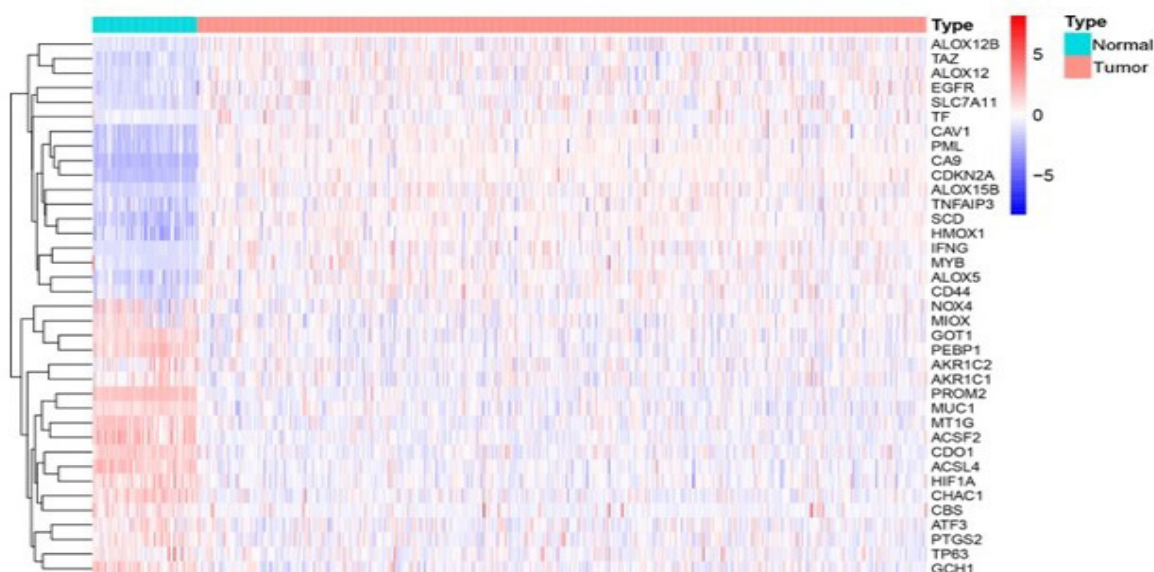


Figure 1. The heatmap of 37 ferroptosis-related DEGs in renal tissue between normal and tumor from TCGA. The red represents up-regulation, whereas the blue represents down-regulation. The columns of the heatmap are samples, and the rows are different genes in the figure.

samples and 72 normal samples were adopted. Founded on reverse Kaplan-Meier (K-M) method, the median follow-up time in the study group was 4.90 years, while the median follow-up time in the control group was 4.41 years. As death status of patients was regarded as the end of our study, the censoring proportion of the training and testing group were 67.3% and 66.5% in KM survival analysis, respectively. The FRGs were obtained from the world's first database of ferroptosis (FerrDb, <http://www.zhounan.org/ferrdb/>) (Supplementary Table S1).⁽¹¹⁾ The FRGs with evidence level of "verified" were included, which required convincing evidence from strict tests such as pharmacological or genetic inhibition or activation tests in humans. All the

data via TCGA and FerrDb were both so publicly available and accessible. Finally, 113 FRGs were included in the study.

The Differentially Expressed FRGs Identification

The differentially expressed genes (DEGs) between tumor tissues and tumor-adjacent normal tissues in the TCGA cohort were identified by combining the expression profile of 113 FRGs using the “limma” R package with a false discovery rate (FDR) < 0.05 and |log₂(fold change)| > 1 considered as statistical significance. The heatmap of the DEGs was drawn using the R package “heatmap”. The TCGA cohort including 502 ccRCC samples was allocated randomly and averagely in the

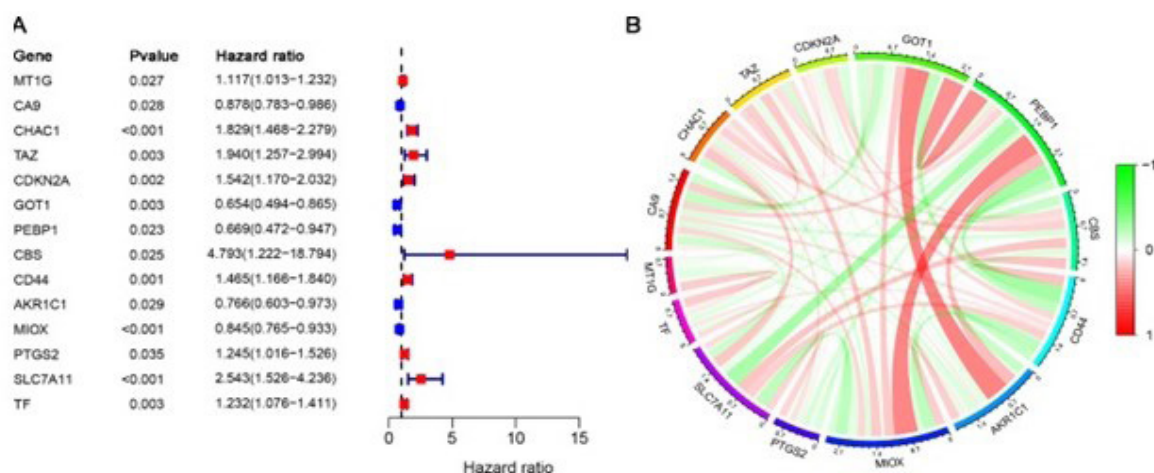


Figure 2. Prognosis and correlation analysis of 14 FRGs. (A) The forest plot of univariable Cox regression analysis between gene expression and OS. The plot displayed the prognostic ability of the fourteen FRGs included in the 37 DEGs. The blue square indicated that the hazard ratio is less than 1, and the red one is greater than 1. And the length of the blue purple line represents the 95% confidence interval. (B) The network showing the correlation of 14 FRGs. The correlation coefficients are represented by green and red line whose depth means the degree of correlation. Red represents positive correlation, while green represents the negative correlation, and each region area of the network figure represents the relative abundance of 14 gene expression profiles.

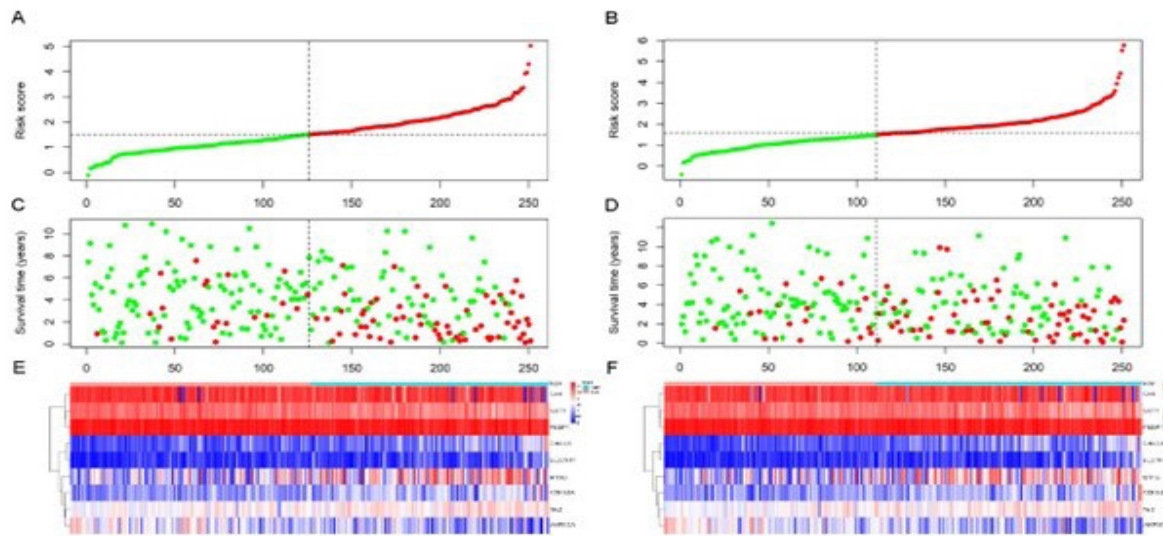


Figure 3. Construction of the 9 FRGs prognostic risk signature model. The group of figures on the left is for the training group (A, C, E), and the other set of figures on the right is for the validation group (B, D, F). (A, B) Risk score distribution curves of ccRCC patients according to the median value. (C, D) The scatter diagram shows that distributions of survival times and status to ccRCC patients between high-risk group and low-risk group in the TCGA cohort. (E, F) Heatmaps of expression for 9 risk genes in the high-risk (blue) and low-risk (pink) group of OS model.

training cohort (n=251) and internal validation cohort (n=251) by using a stratified random split in the R package “caret”. Then, based on these DEGs, the prognosis-related FRGs were obtained by univariable Cox analysis in the training cohort. Finally, the correlation of prognosis FRGs was analyzed by R package “corrplot” based on Pearson method.

A Model of Prognostic FRGs Signature Construction and Evaluation

To identify the independent risk prognostic genes and build an optimal prognostic model, multivariable Cox regression analysis was utilized to identify FRGs signature based on the lowest Akaike information criterion (AIC) value to by forward and backward stepwise regression method. The normalized expression matrix of candidate ferroptosis-related prognostic DEGs was treated as an independent variable and OS and status of patients in the training cohort as a response variable. The prognostic risk score of the ccRCC patients was calculated based on a linear combination of the regression coefficients and the normalized expression level of gene expression. The calculation formula used for the analysis was as follows:

$$\text{Risk score} = \sum_{i=1}^n \text{Coef}_i \times \text{Exp}_i$$

Where Coef_i represents the corresponding regression coefficient, Exp_i is the value of each gene's expression. According to the median value of the risk score in the training cohort and validation cohort, the patients of the training and validation cohorts all were classified into high-risk and low-risk groups. To observe whether the high- and risk-group can be divided based on the expression of modeling FRGs in order to explore the difference between two risk groups form expression, principal component analysis (PCA) was carried out using the R package “scatterplot3d” in the training and

validation cohort. Then, we transformed variables into 3 principal components by the dimension reduction. For the survival analysis of each gene, the survival curves were plotted by KM method. The time-dependent ROC curve was plotted to calculate the area under the ROC curve and evaluate the predictive power of the prognostic model founded on signatures at 1-, 3-, and 5-year survival.

Prognostic Predictive Nomogram Construction and Validation

Univariable and multivariable Cox regression analyses were applied to assess whether prognostic riskscore was independent of other clinical features of ccRCC and to screen for independent prognostic factors, which can verify further the prognostic value of riskscore model. A prognostic predictive nomogram was established by multivariable Cox regression to forecast 1-, 3-, and 5-year OS of ccRCC patients in the TCGA, including all prognostic parameters. Meanwhile, we calculated the calibration plot, the Harrell's C-index, and AUC of the ROC curve for the nomogram to evaluate the accuracy and power of the nomogram, whose analysis was performed using the R package. The C-index could be contributed to assess the consistency between the actual outcome frequencies and the model prediction probabilities. Besides, another predictor for 5-year OS was evaluated by ROC values, such as risk score, age, grade, and stage.

Function Enrichment and Immune Status Analysis

According to the 50% probability value of the nomogram predicted in the 5-year OS, the ccRCC patients of TCGA were divided into two groups. The 5-year OS probability of the high-OS group was greater than 50%, and the 5-year OS probability of the low-OS group was less than 50%. The genes with greater or equal to 1 in

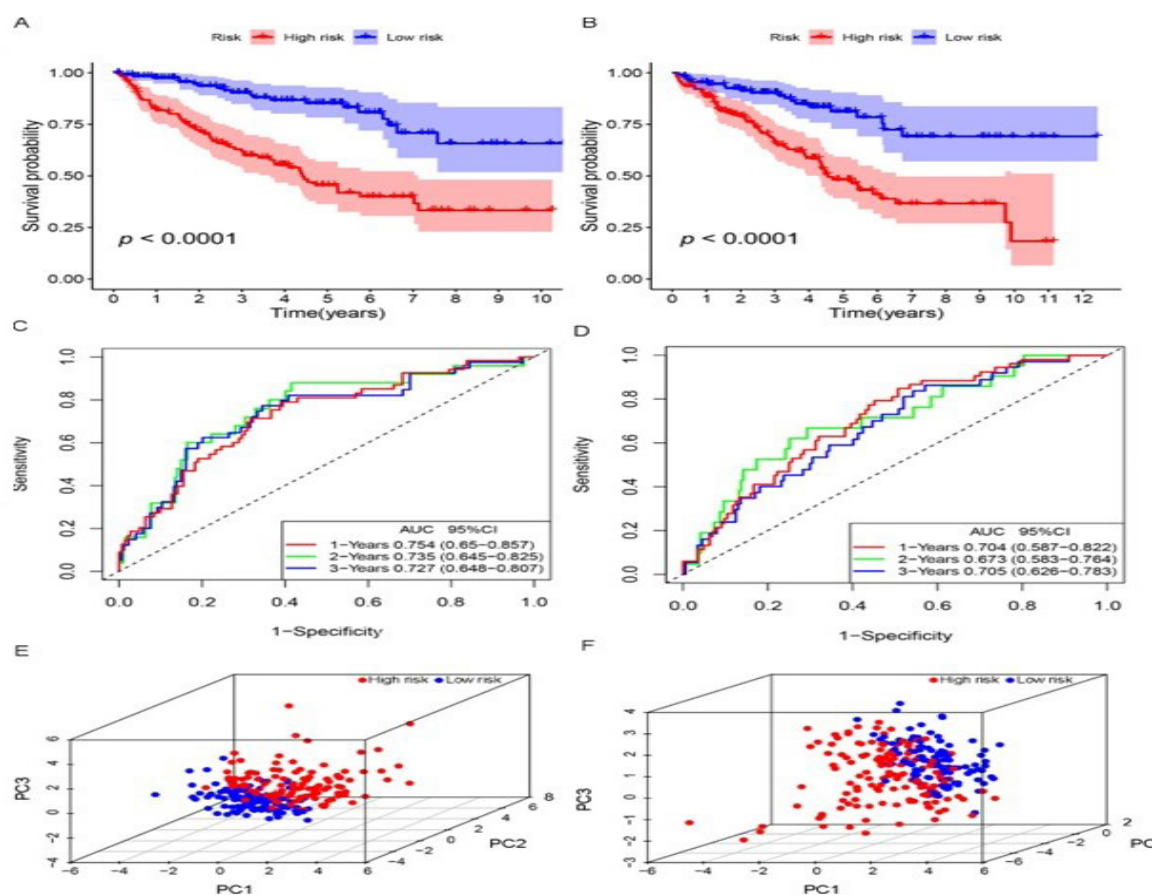


Figure 4. Prognostic analysis and validation of the 9-gene ferroptosis-related signature model in the TCGA cohort. The group of figures on the left is for the training group (A, C, E), and the other set of figures on the right is for the validation group (B, D, F). (A-B) The Kaplan-Meier survival curves of the high-risk and low-risk group in the train set and validation set. (C-D) ROC curve was used to evaluate the prediction efficiency of the prognostic signature in the train set and validation set. (E-F) PCA scatter plot of ferroptosis-associated genes between high- and low-risk groups. The legend indicates the color of the different risk: red, high risk; blue, low risk.

2-fold change ($|\log_2FC| \geq 1$) and $FDR \leq 0.05$ were considered the threshold of DEGs between the 5-year low-OS and high-OS group. These DEGs were visualized by the volcano plot. And the "clusterProfiler" R package was used by conducting Gene Ontology (GO) and Kyoto Encyclopedia of Genes and Genomes (KEGG) analyses for the DEGs. The ssGSEA was applied to evaluate the infiltrating score of immune cells and the immune-related pathways or functions activity. And the relevant supplementary **table 2** included the annotated gene set file. The ssGSEA scores of immune cells and pathways or functions between the 5-year low-OS and high-OS group were compared by the Wilcoxon test. All statistical data were analyzed by R software (Version 4.0.2) for Windows. The results with $P < 0.05$ were considered statistically significant, and all reported P values were two-tailed.

Statistical Analysis

The clinical features between the training and validation cohorts used the Chi-squared to compare their discrepancy. The OS between different risk groups was contrasted using the log-rank test. The ssGSEA scores of immune cells and pathways or functions between 5-year low-OS and high-OS group were compared by the Wilcoxon rank-sum test. All statistical data were analyzed

by R software (Version 4.0.2) for Windows. The results with $P < 0.05$ were considered statistically significant, and all reported P values were two-tailed.

RESULTS

Screening for prognostic FRGs in the ccRCC patients. The 37 DEGs of 113 FRGs were identified between 502 ccRCC tumor tissues and 72 normal renal tissues in the TCGA-KIRC dataset, among which 18 genes were up-regulated and 19 genes were down-regulated. The heatmap of the 37 DEGs was constructed in **Figure 1**. According to the principle of random allocation and 1:1 equal allocation, we divided 502 patients into a training group and a verification group, with 251 cases in each group. The detailed clinicopathological features of these patients have been summarized in **Table 1**, including gender, age, grade, stage, and status. By the Chi-squared, the P values of all features were all greater than .05, which indicated that Baseline clinicopathological feature had no statistical difference between the training group and the validation group. Furthermore, we performed the univariable Cox regression analysis for the expression of DEGs of training cohort to better understand the prognostic role of DEGs in ccRCC patients. The result of forest plot showed that MT1G,

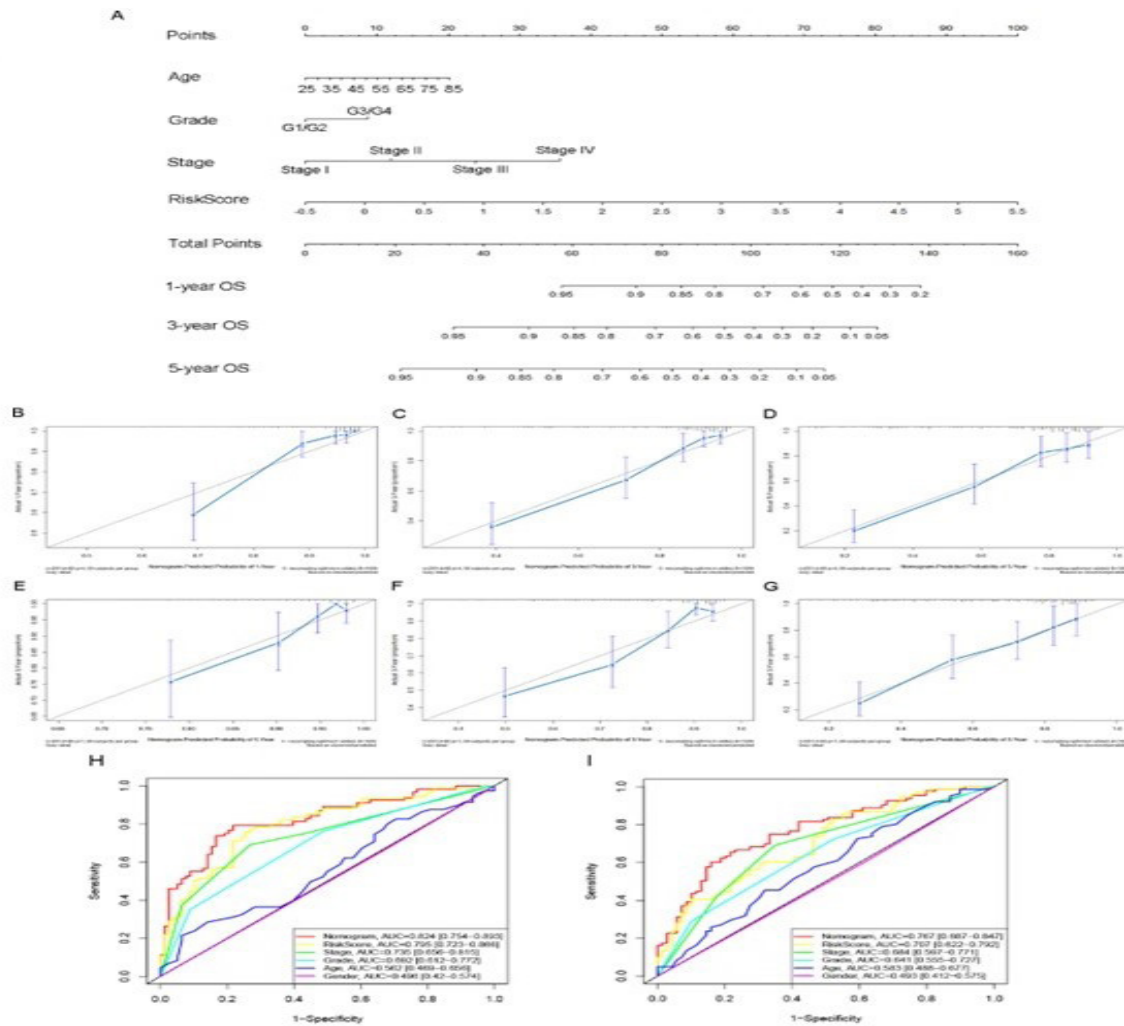


Figure 5. Construction and validation of the nomogram model to predict OS of ccRCC patients in the TCGA dataset. **(A)** Nomogram based on age, grade, stage, and risk score, was used to predict the 1-, 3- and 5-year survival probability of ccRCC patients in the training cohort. The calibration curves of the nomogram showed the OS probability of prediction at 1-, 3-, and 5-year in the TCGA training cohort **(B-D)** and validation cohort **(E-G)**. The time-dependent ROC curves for the 5-year OS nomogram, risk score, stage, grade, age and gender in the training cohort **(H)** and validation cohort **(I)**.

CHAC1, TAZ, CDKN2A, CBS, CD44, PTGS2, SLC7A11, and TF were risk factors with HR (Hazard ratio) > 1, while CA9, GOT1, PEBP1, AKR1C1, and MIOX were protective factors with HR < 1 in ccRCC patients (p value < .05 in 14 genes) **(Figure 2A)**. The correlation and interaction between these genes were presented in Figure 2B, which indicated that three pairs of positive genes were more related than others, including GOT1 and AKR1C1, GOT1 and PEBP1, MIOX and PEBP1.

Construction and validation of a prognostic model

A prognostic model basing the expression profile of the 14 genes was established by the multivariable Cox regression analysis, which identified the 9-gene signature (MT1G, CA9, CHAC1, TAZ, CDKN2A, GOT1, PEBP1, AKR1C1, SLC7A11). And then we obtained the risk score calculation formula as follows: risk-score= $0.10^3 \times$ expression value of MT1G + $(-0.228 \times$ expression value of CA9) + $0.333 \times$ expression value of CHAC1 + $0.493 \times$ expression value of TAZ + $0.285 \times$ expression value of CDKN2A + $(-0.376 \times$ expression

value of GOT1) + $0.377 \times$ expression value of PEBP1 + $(-0.276 \times$ expression value of AKR1C1) + $0.751 \times$ expression value of SLC7A11. The patients were divided into high- and low-risk groups by median value of risk model scoring formula in the training and validation cohort **(Figure 3A-3B)**. Both the training and validation groups showed significantly higher mortality rates in the high-risk group than in the low-risk group (Figure 3C-3D). The heatmap displayed that the expression of the 9 risk signatures was consistent in the training and validation groups **(Figure 3E-3F)**. Our study found that high-risk ccRCC patients had a significantly worse OS than those in the low-risk counterparts from KMsurvival curves basing the risk score **(Figure 4A-4B)**. And the time-dependent ROC curves demonstrated that the risk model basing 9-gene signature harbored a positive ability to predict OS in the training and validation groups, and the AUC of training cohort reached 0.754 at 1 year (95%CI, 0.650-0.857), 0.735 at 2 years (95%CI, 0.645-0.825), and 0.727 at 3 years (95%CI, 0.648-0.807), and the AUC reached 0.704 at 1 year (95%CI, 0.587-0.822),

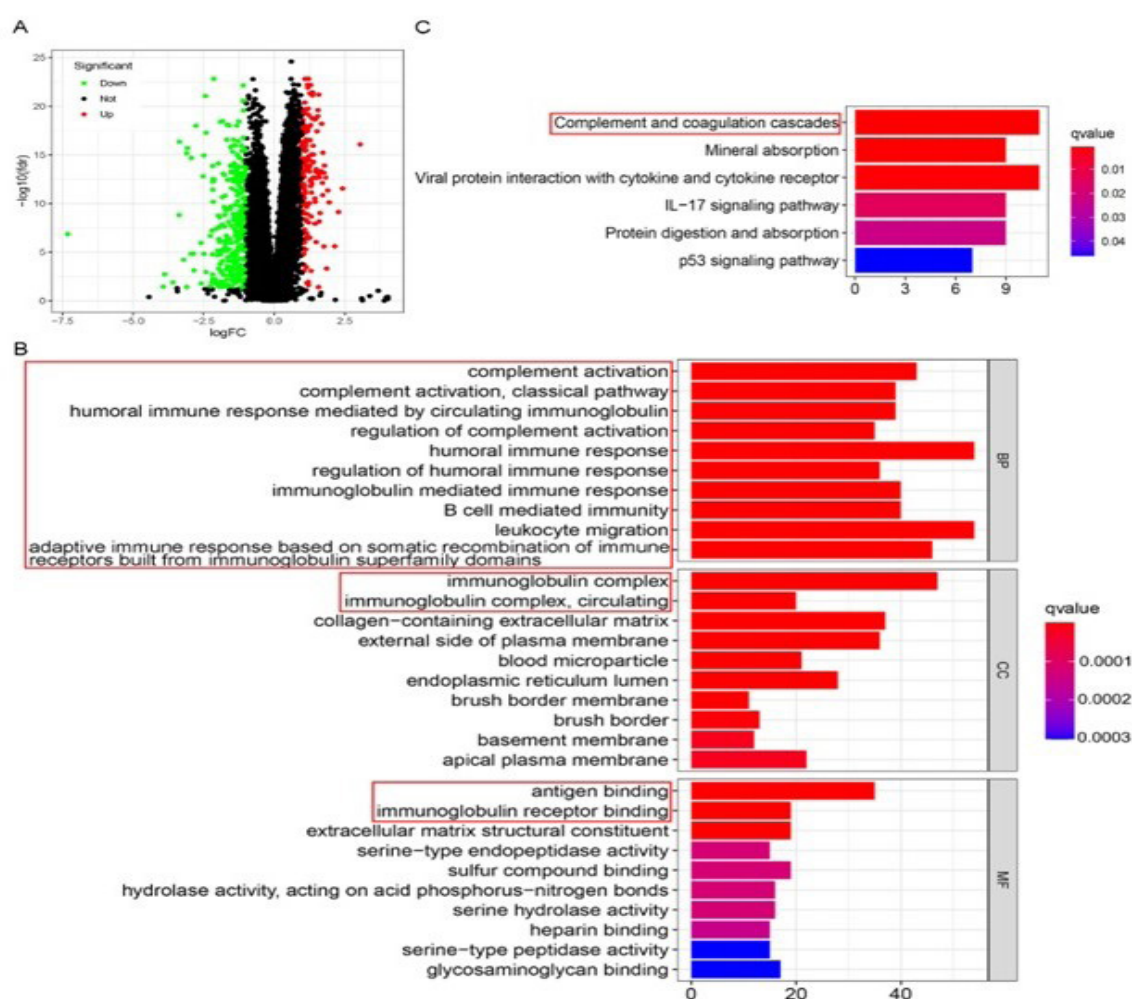


Figure 6. Functional enrichment analysis of DEGs between the high-OS and low-OS groups. The volcano plot on the upper left (A) is the result of the DEGs of two different OS groups, and the red is up-regulation of gene expression and the green is down-regulation of gene expression. Rectangles is shown that the most significant GO enrichment (B) and KEGG pathways (C) based on the DEGs. The color represents q-value and the length of abscissa represents count. The red rectangles highlight the overlap of the immune-related pathways.

00.673 at 2 years (95%CI, 0.583-0.764), and 0.705 at 3 years (95%CI, 0.626-0.783) in the validation cohort (Figure 4C-4D). Finally, PCA analysis was performed and confirmed that patients in high- and low-risk groups were distributed in discrete directions to indicate the difference of risk groups (Figure 4E-4F).

Independent prognostic predictors evaluation of the 9-gene signature

The univariable and multivariable Cox proportional regression analysis was performed to evaluate whether the 9-gene risk signature can consider as an independent decisive factor of OS with ccRCC patients in the training cohort. As shown in Table 2, univariable Cox analysis revealed that the risk score was significantly associated with shorter OS (95% CI: 2.10–3.52; HR: 2.72; $P < .001$), as was multivariable Cox analysis (95% CI: 1.58–2.80; HR: 2.11; $P < .001$), which indicated that the risk score served as one of the independent prognostic factors. In addition, grade (G3/G4) and stage (III, IV) were significantly correlated with poor survival of ccRCC patients in the other clinicopathologic variables of univariable analysis. Interestingly, stage IV was also

an independent prognostic risk factor.

Constructing and validating the predictive nomogram

Further, we established a nomogram and used it to predict the probability of 1-year, 3-year, and 5-year OS in the ccRCC patients from the training cohort (Figure 5A). Four prognostic predictors of age, grade, stage, and risk score were included in the nomogram. The C-index of the nomogram for OS was 0.790 (95% CI, 0.740-0.840) in the training cohort and 0.765 (95% CI, 0.714-0.816) in the validation cohort, whose results showed that nomogram had a stable and accurate predictive power. According to the nomogram calibration curve evaluation, it showed that the OS predicted to value the matches well with the actual value and wonderful prediction performance, especially the prediction performance of 5-year OS (Figure 5B-5G). In addition, we also drew the ROC curve based on the nomogram, riskScore, Stage, Grade, Age, and Gender. The AUC values for training set nomogram, riskscore, stage, grade, age, and gender were respectively 0.824, 0.795, 0.735, 0.692, 0.562, 0.496, while AUC values of vali-

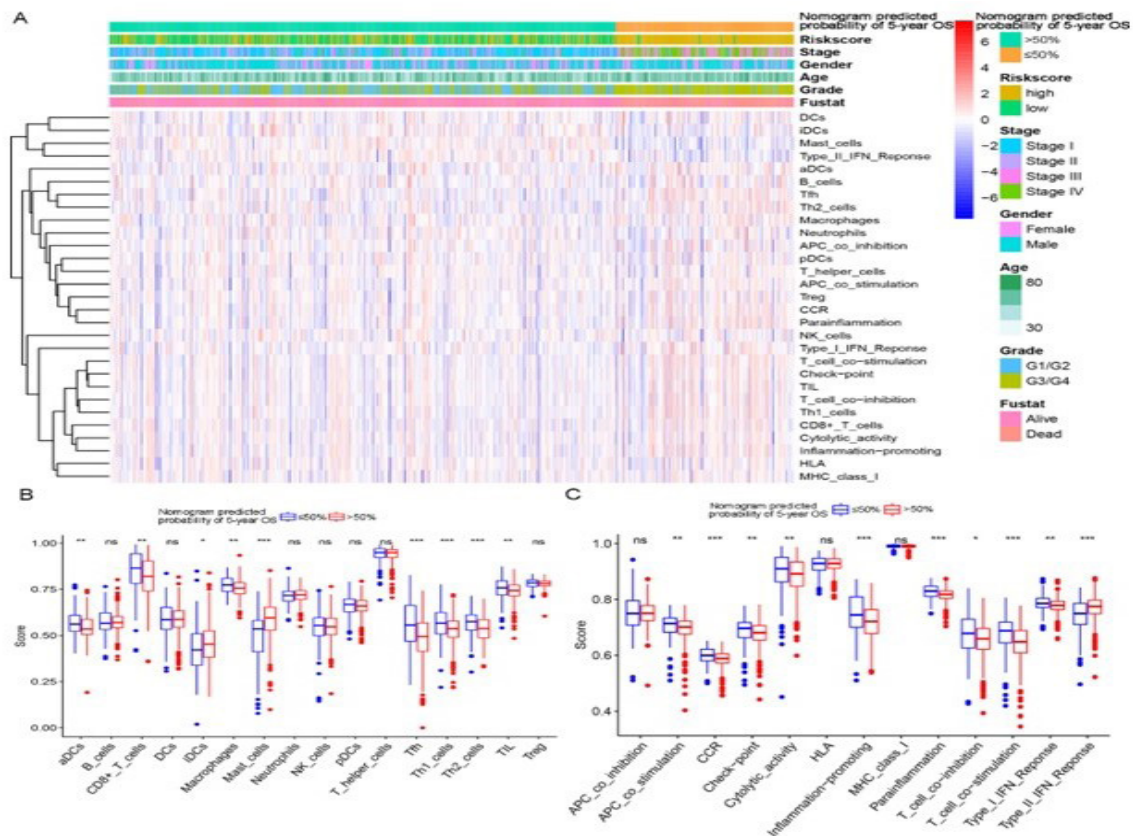


Figure 7. The ssGSEA analysis of different immune status between 5 year high-OS group and low-OS group. (A) The heatmap showed that the score of immune cell and immune-related pathways or functions in the ccRCC patients of high-OS group (green) and low-OS group (orange). The color of different clinicopathological parameters are shown as annotations, while the immune status scores is also indicated by a color bar. Green means low score and red means high score. (B-C) The scores of 16 immune cells (B) and 13 immune-related functions (C) of the high- (blue) and low- (red) OS groups are revealed in these boxplots.

dation set were respectively 0.767, 0.707, 0.684, 0.641, 0.583, and 0.495 (Figure 5H-5I). It is shown that the prediction ability of nomogram was best in the ccRCC patients.

Functional analysis of DEG between the low- and high-OS groups

Using the nomogram to evaluate the 5-year OS probability of all ccRCC patients in TCGA, we obtained a median of 50% probability of 5-year survival to divide into the high- and low-OS group in the ccRCC patients. The R package “limma” was used to identify 468 DEGs between the high- and the low-OS group, including 150 up-regulated genes and 318 down-regulated genes (Figure 6A). GO and KEGG enrichment analyses were performed to investigate the potential biological function and pathway in these DEGs. In the biological process (BP), the enrichment of DEGs was the highest in the complement activation pathway. It is interesting that the enrichment of the first ten BP is related to the immune pathway. In cell composition (CC), the enrichment factor of immunoglobulin complex is the highest, while the antigen-binding enrichment is the highest in terms of molecular function (MF) (Figure 6B). Meanwhile, the KEGG analysis showed that the main enrichment processes are complement and coagulation cascades pathway, mineral absorption, and viral protein interaction with cytokine and cytokine receptor pathway (Figure 6C). The red rectangle of GO and

KEGG pathway analysis plot revealed that the DEGs of high- and low-OS groups were mainly enriched in pathways of immune-related biological processes.

Immune status in the low- and high-OS groups

Finally, we further explored the immune status by quantifying the enrichment levels of different immune cell subtypes, functions, or pathways with ssGSEA score in ccRCC. The 16 immune cells and 13 immune-related function scores were obtained and analyzed in the discovery set using ssGSEA. Overall, the distribution of immune status was different between the 5-year high- and low-OS groups, with most of the immune cell and immune-related pathways or function scores higher in the low-OS group than the high-OS group (Figure 7A). It is shown that aDCs, CD8+ T cells, macrophages, Follicular helper T cell (Tfh), helper T cells (Th1 and Th2), and TIL infiltration were higher in the 5-year low-OS group ($p < 0.05$), while iDCs and mast cells infiltration were higher in the 5-year high-OS group ($p < 0.05$) (Figure 7B). Among them, CD8+ T cells, T helper cells, TIL, and macrophages are the most common immune cell populations in the ccRCC patients. Interestingly, according to the expression of immune function (Figure 7C), only the score of type II IFN response in the high-OS group is significantly higher than in the low-OS group. However, the type I IFN response in the high-OS group is lower than in the low-OS group. The immune scores of MHC class I, cytolitic-activity,

and HLA are highest in the function enrichment.

DISCUSSION

The development of ccRCC is strongly associated with the loss of the VHL gene, loss of chromosome 3p, and the occurrence of extrachromosomal mutational events.⁽¹²⁾ According to the TNM stage, the 5-year survival rate can reach 80% to 90% for patients with early stage I and II ccRCC, while it is around 60% for stage III, and less than 10% for patients with advanced stage IV ccRCC.⁽¹³⁾ Meanwhile, the 5-year survival rate for metastatic ccRCC patients is between 10% and 20%.⁽¹²⁾ Therefore, it is important and urgent to explore the biomarkers and therapeutic targets of ccRCC.

In this study, we systematically investigated the 113 FRGs expression profile of the tumor and normal tissues for ccRCC patients from the TCGA database, as well as the association of FRGs with OS to construct a novel ferroptosis-related prognostic gene risk signature. Nine risk signatures (MT1G, CA9, CHAC1, TAZ, CDKN2A, GOT1, PEBP1, AKR1C1, SLC7A11) were obtained by the univariable and multivariable Cox regression analysis to contribute a new prognostic model in the training cohort. Then, a new nomogram combining the ferroptosis-related riskscore model and clinical features was developed in ccRCC patients. Based on the ROC curve, the predictive efficiency of nomogram for the 5-year OS group was the best (AUC=0.813 in the training cohort; AUC=0.790 in the validation cohort). In addition, the predictive ability of riskscore is better than tumor stage and histological grade. What's more, compared with WU's prediction performance (AUC=0.73) of the survival model on ccRCC FRGs, our risk signature performed similar reliable and accurate.⁽¹⁴⁾ To explore the difference between high- and low-OS groups ccRCC patients, DEGs functional enrichment analyses showed that immune-related pathways were highly enriched in the GO and KEGG analysis, which proclaims that there is a close relationship between ferroptosis and tumor immunity. Further demonstrated by ssGSEA, tumor tissue had different degrees of immune cell subsets infiltration, with the immune cell and immune-related pathways or functions score was significantly different between high- and low-OS groups in ccRCC patients. The prognostic risk gene signature model was composed of 9 FRGs (MT1G, CA9, CHAC1, TAZ, CDKN2A, GOT1, PEBP1, AKR1C1, SLC7A11). Based on the FerrDb database including experimental evidence, the related mechanisms between these genes and ferroptosis processing have been confirmed by published experimental papers in some tumors, of which five of prognostic model genes (CHAC1, TAZ, CDKN2A, GOT1, PEBP1) have been proved to promote ferroptosis by validated experiments, while another four genes (MT1G, CA9, AKR1C1, SLC7A11) inhibit ferroptosis.⁽¹¹⁾ Besides, Wu et al. and Chang et al. also used FRGs to construct a prognostic model in ccRCC, including GOT1 and SLC7A11.^(14,15) Therefore, GOT1 and SLC7A11 may be considered as important signatures in ccRCC. As a component of the cystine/glutamate antiporter and target of p53, SLC7A11 was up-regulated to increase cystine intake and inhibit ROS-induced ferroptosis when p53 was knocked down.⁽¹⁶⁾ Furthermore, SLC7A11 overexpression had been closely associated with poor prognosis in several cancers, while knock-down of SLC7A11 can hinder cancer proliferation,

invasion, and metastasis by participating in several pathways, including the regulation of oxidative stress and immune regulation.⁽¹⁷⁾ CDKN2A, a tumor suppressor gene, partook in the modulation of ferroptosis by the p53-dependent and a p53-independent manner when CDKN2A was activated, and both processes were closely related to SLC7A11.⁽¹⁸⁾ The involvement of the p53 pathway was also mentioned in the KEGG analysis. A study showed that ccRCC patients had a significantly worse prognosis when CDKN2A was mutated.⁽¹⁹⁾ Downregulation of MT1G in ccRCC patients may render tumor cells growth-arrested, induce apoptosis, and promote promoter methylation, which is similar to the role downregulating MT1G inducing ferroptosis.^(20,21) As a metalloenzyme, CA9 has been reported to contribute to ferroptosis through iron overload and trigger lipid peroxidation when it was knocked down under hypoxia in malignant mesothelioma cells.⁽²²⁾ The high expression of CA9 is related to good outcomes and can be used as a prognostic biomarker for ccRCC.⁽²³⁾ Pertinent mechanisms of other genes affecting the prognosis of ccRCC through ferroptosis remain to be clarified by more experiments.

Immunotherapy has gradually become a new clinical strategy for cancer treatment, especially for ccRCC. However, more effective targets are needed for immunotherapy of ccRCC, and the potential regulation among targets still needs to be supplemented. Based on GO analysis and KEGG analysis, we found unsurprisingly that the first ten enrichment pathways of BP, the first two enrichment pathways of CC and MF, and the first pathway of KEGG are all related to immune pathways, which mainly touch upon complement pathway, humoral and cellular immune response, metabolism of immune complexes, immune biological processes related to immunoglobulin pathway. According to the ssGSEA score, the antigen presentation process (including the score of aDCs, iDCs, macrophages, and APC co-stimulation) was significantly different between the 5-year low-OS and high-OS group. In another study, it was found that early ferroptosis has immunogenicity and can promote the maturation of bone-marrow derived dendritic cells, thus promoting the immune response to enhance tumor immunity, whether in vivo or vitro.⁽²⁴⁾ And a recent study reported that ferroptosis-related cells were also swallowed and cleared by macrophage in vitro human monocyte-derived macrophages culture, like apoptosis, because ferroptosis cells may release phosphatidylserine to induce macrophage phagocytosis themselves.⁽²⁵⁾

Interestingly, the high infiltration of CD8+ T cells was located in the low-OS group of our study. As Braun et al reported, the high infiltration of CD8+ T cells was also associated with a poor prognosis in ccRCC patients.⁽²⁶⁾ Activation of immunotherapy increased CD8+ T cells, which promoted lipid peroxidation and ferroptosis of tumor cells by releasing interferon-gamma (IFN γ) and downregulating SLC7A11 and SLC3A2.⁽²⁷⁾ However, increased expression of CD36 in tumor-infiltrating CD8+ T cells induced ferroptosis, resulting in decreased cytotoxic cytokines and loss of antitumor activity of CD8+ T cells.⁽²⁸⁾ Therefore, the mechanism of action between ccRCC immune infiltration of CD8+ T cells and ferroptosis requires elucidation from further experiments. Meanwhile, a higher response of the type II IFN and a lower immune score of check point were

shown in the 5-year high-OS group. It is proved by the experiments that blocking checkpoint was conducive to enhance the ferroptosis process by increasing the release of IFN γ .⁽²⁷⁾ GPX4 is essential for T cell immunity expansion and promotes maintenance of CD8⁺ T cells.⁽²⁹⁾ In the previous study, the glutathione metabolic system carried a big weight in ccRCC.⁽¹²⁾ And GPX4 of glutathione metabolic system has been advised as a treatment target of ccRCC patients, but there is no reliable and safe ferroptosis therapy in clinic.⁽³⁰⁾ Therefore, ferroptosis-related immunotherapy is expected to become a new clinical treatment strategy for ccRCC. Nevertheless, there are some limitations to our current study. First, we established and validated the prognostic model only with the expression profile of ccRCC in retrospective data from TCGA. This requires prospective cohort studies to validate this prognostic model. Second, it should be noted that founded on univariable Cox regression, the possibility of sparse-data bias occurred in the patients with stage IV in order to lead to the risk bias of exaggeration in a relevant HR and confidence interval. Besides, the mechanism and pathway of ferroptosis in ccRCC patients still need to be further explored. Ultimately, even though 9 FRGs novel genes are significantly related to the survival of ccRCC patients and become new treatment targets possibly, the relationship among FRGs, riskscore and immune activity needs to be further constructed for an exact connection and validation through more experiments.

CONCLUSIONS

In summary, our study established a novel prognostic model of 9 FRGs risk signatures and promising prognostic nomogram for ccRCC patients, and validated its reliability successfully. Our study provided an accurate and reliable prediction efficiency and an individualized treatment strategy to ccRCC patients. Furthermore, our study may help researchers to probe the possible biological mechanisms between tumor immunity and ferroptosis in ccRCC.

CONFLICTS OF INTEREST

All authors declare that they have no conflict of interest with the state. All authors have completed the ICMJE uniform disclosure form.

ACKNOWLEDGEMENT

The present study was supported by the National Key Research and Development Program of China (contract No. 2018YFA0902801), National Natural Science Foundation of China (contract No. 81803576), Guangdong Basic and Applied Basic Research Foundation (contract No. 2020A1515010152), Public health research project in Futian District, Shenzhen (contract no. FTWS2020026), the research start-up fee for the Eighth Affiliated Hospital, Sun Yat-sen University (contract no. zdbykyqdf005), and the Sixth Clinical College of Guangzhou Medical University (contract No.2020ALY05).

SUPPLEMENTARY MATERIALS

Supplementary Table S1 is the acquisition of validated ferroptosis-genes' names and associated information from the FerrDb database. Supplementary Table S2 is related data information for ssGSEA. Supplementary

Figure S1 shows the study design flow.

APPENDIX

<https://journals.sbmu.ac.ir/urolj/index.php/uj/libraryFiles/downloadPublic/38>

REFERENCES

1. Hsieh JJ, Purdue MP, Signoretti S, et al. Renal cell carcinoma. *Nat Rev Dis Primers*. 2017;3:17009.
2. Capitanio U, Bensalah K, Bex A, et al. Epidemiology of Renal Cell Carcinoma. *Eur Urol*. 2019;75:74-84.
3. Vuong L, Kotecha RR, Voss MH, Hakimi AA. Tumor Microenvironment Dynamics in Clear-Cell Renal Cell Carcinoma. *Cancer Discov*. 2019;9:1349-57.
4. Majer W, Kluzek K, Bluysen H, Wesoly J. Potential Approaches and Recent Advances in Biomarker Discovery in Clear-Cell Renal Cell Carcinoma. *J Cancer*. 2015;6:1105-13.
5. Stockwell BR, Friedmann Angeli JP, Bayir H, et al. Ferroptosis: A Regulated Cell Death Nexus Linking Metabolism, Redox Biology, and Disease. *Cell*. 2017;171:273-85.
6. Dixon SJ, Lemberg KM, Lamprecht MR, et al. Ferroptosis: an iron-dependent form of nonapoptotic cell death. *Cell*. 2012;149:1060-72.
7. Gao M, Yi J, Zhu J, et al. Role of Mitochondria in Ferroptosis. *Mol Cell*. 2019;73:354-63 e3.
8. Lippmann J, Petri K, Fulda S, Liese J. Redox Modulation and Induction of Ferroptosis as a New Therapeutic Strategy in Hepatocellular Carcinoma. *Transl Oncol*. 2020;13:100785.
9. Xu T, Ding W, Ji X, et al. Molecular mechanisms of ferroptosis and its role in cancer therapy. *J Cell Mol Med*. 2019;23:4900-12.
10. Miess H, Dankworth B, Gouw AM, et al. The glutathione redox system is essential to prevent ferroptosis caused by impaired lipid metabolism in clear cell renal cell carcinoma. *Oncogene*. 2018;37:5435-50.
11. Zhou N, Bao J. FerrDb: a manually curated resource for regulators and markers of ferroptosis and ferroptosis-disease associations. *Database (Oxford)*. 2020;2020.
12. Hsieh JJ, Le VH, Oyama T, et al. Chromosome 3p Loss-Orchestrated VHL, HIF, and Epigenetic Deregulation in Clear Cell Renal Cell Carcinoma. *Journal of clinical oncology : official journal of the American Society of Clinical Oncology*. 2018;36:Jco2018792549.
13. Jonasch E, Gao J, Rathmell WK. Renal cell carcinoma. *BMJ*. 2014;349:g4797.
14. Wu G, Wang Q, Xu Y, Li Q, Cheng L. A new survival model based on ferroptosis-related genes for prognostic prediction in clear cell renal cell carcinoma. *Aging*. 2020;12:14933-48.
15. Bai D, Feng H, Yang J, et al. Genomic analysis uncovers prognostic and immunogenic characteristics of ferroptosis for clear cell renal cell carcinoma. *Molecular Therapy - Nucleic Acids*. 2021.
16. Jiang L, Kon N, Li T, et al. Ferroptosis as a p53-mediated activity during tumour

- suppression. *Nature*. 2015;520:57-62.
17. Lin W, Wang C, Liu G, et al. SLC7A11/xCT in cancer: biological functions and therapeutic implications. *Am J Cancer Res*. 2020;10:3106-26.
 18. Chen D, Tavana O, Chu B, et al. NRF2 Is a Major Target of ARF in p53-Independent Tumor Suppression. *Mol Cell*. 2017;68:224-32 e4.
 19. Feng C, Sun Y, Ding G, et al. PI3Kbeta inhibitor TGX221 selectively inhibits renal cell carcinoma cells with both VHL and SETD2 mutations and links multiple pathways. *Sci Rep*. 2015;5:9465.
 20. Si M, Lang J. The roles of metallothioneins in carcinogenesis. *J Hematol Oncol*. 2018;11:107.
 21. Sun X, Niu X, Chen R, et al. Metallothionein-1G facilitates sorafenib resistance through inhibition of ferroptosis. *Hepatology*. 2016;64:488-500.
 22. Li Z, Jiang L, Chew SH, et al. Carbonic anhydrase 9 confers resistance to ferroptosis/apoptosis in malignant mesothelioma under hypoxia. *Redox Biol*. 2019;26:101297.
 23. Bui MH, Seligson D, Han KR, et al. Carbonic anhydrase IX is an independent predictor of survival in advanced renal clear cell carcinoma: implications for prognosis and therapy. *Clin Cancer Res*. 2003;9:802-11.
 24. Efimova I, Catanzaro E, Van der Meeren L, et al. Vaccination with early ferroptotic cancer cells induces efficient antitumor immunity. *J Immunother Cancer*. 2020;8.
 25. Kloditz K, Fadeel B. Three cell deaths and a funeral: macrophage clearance of cells undergoing distinct modes of cell death. *Cell Death Discov*. 2019;5:65.
 26. Braun DA, Hou Y, Bakouny Z, et al. Interplay of somatic alterations and immune infiltration modulates response to PD-1 blockade in advanced clear cell renal cell carcinoma. *Nat Med*. 2020;26:909-18.
 27. Wang W, Green M, Choi JE, et al. CD8(+) T cells regulate tumour ferroptosis during cancer immunotherapy. *Nature*. 2019;569:270-4.
 28. Ma X, Xiao L, Liu L, et al. CD36-mediated ferroptosis dampens intratumoral CD8(+) T cell effector function and impairs their antitumor ability. *Cell Metab*. 2021;33:1001-12.e5.
 29. Matsushita M, Freigang S, Schneider C, et al. T cell lipid peroxidation induces ferroptosis and prevents immunity to infection. *J Exp Med*. 2015;212:555-68.
 30. Zou Y, Palte MJ, Deik AA, et al. A GPX4-dependent cancer cell state underlies the clear-cell morphology and confers sensitivity to ferroptosis. *Nat Commun*. 2019;10:1617.